AN EVALUATION OF THE PHYSICAL PROPERTIES OF ND:YAG LASER WELDED HIGH STRENGTH 6000 SERIES ALUMINUM ALLOYS

Barry R. Leigh
Bombardier Aerospace, Toronto ON M3K 1Y5
Cheung Poon
National Research Council Canada, Ottawa ON K1A 0R6
Hugh W. Kerr and W.H.S. Lawson
University of Waterloo, Waterloo ON N2L 3G1
Norman Ferguson
Ryerson Polytechnic University, Toronto, ON M5B 2K3

Keywords: laser welding, 6000 series aluminum alloys, weld defects

Abstract

Recent advances in high powered laser technology have made it possible to consider welded airframe primary structure in commercial aircraft. Potential advantages include incremental weight and manufacturing cost reductions and improved corrosion resistance. In this paper, some of the potential defects in aluminum laser welds are discussed. In addition, the results of the examination of some early weldments made with aluminum alloy 6013 and several filler alloys are presented. The significance of these findings is discussed.

1. Introduction

The recent commercial availability of high powered lasers has made it possible to consider welding as a practical alternative to riveting in the assembly of commercial aircraft structures. In compression dominated areas, such as the lower fuselage, the welded structure may be on the order of 10% lighter due the more efficient use of stringer material, the favorable yield strength of candidate weldable alloys and the reduction of the amount of sealant and the number of fasteners. The inherent corrosion resistance of these weldable alloys and the elimination of moisture traps between faying surfaces will result in reduced maintenance and repair costs. Laser welded joints are produced at rates up to 10m/min., on the order of 100 times faster than automatic riveting machines. This will result in significant reductions in manufacturing costs.

The Al-Mg-Si-Cu alloys 6013 (Alcoa) and 6056 (Pechiney) have been selected for investigation because of their strength, formability and weldability. These alloys are used in the same application by EADS (Airbus) and have been successfully used by Bombardier Aerospace in other structural applications.

The 6000 series aluminum alloys exhibit a tendency to solidification cracking unless the weld metal composition includes appropriate filler metal additions. Intergranular cracking in partially melted base metal adjacent to the weld fusion boundary (liquation cracking) is also a known problem in 6000 series arc welds.

The peak temperature in the heat affected zone (HAZ) will cause varying amounts of grain coarsening and solution of the precipitates responsible for strengthening 6000 series alloys. Moreover, local as-welded microstructural features can be expected that may reduce intergranular corrosion resistance. However, it is believed that a partial recovery of weldment strength and corrosion resistance will result from welding in the naturally aged condition, followed an artificial aging heat treatment of the welded assembly.

Excessive porosity in aluminum welds can result unless positive measures are taken to keep sources of hydrogen, such as moisture or organic compounds, away from the weld zone. Porosity

may also result from poor control of laser welding process parameters.

In the present work, examination of preliminary test weldments has emphasized study of the significance of the main postulated difficulties with weld soundness and properties.

2. Metallurgical Issues

Because of the typically large and steep variation of strength across an aluminum weldment, conventional cross-weld tensile tests are not a sensitive indicator of local properties in the weld or HAZ. Low-load hardness testing using a conical or pyramidal indenter (e.g. Vickers hardness test) has been used as a way of mapping local mechanical properties across a weld. A wide variety of empirical corrections has been developed to relate hardness to strength. A good compilation of these can be found in Vander Voort [1]. More recently, Grong [2] has determined hardness-strength correlation data specifically for precipitation-hardened aluminum alloys.

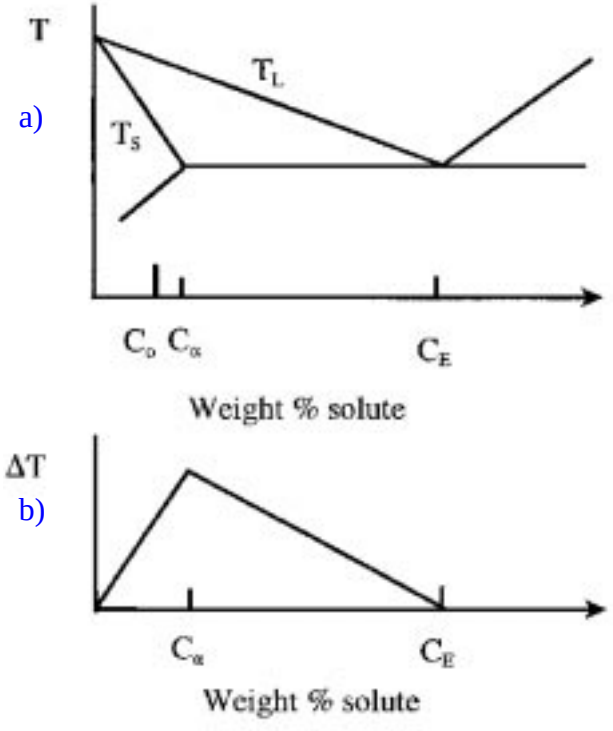

Fig. 1 Solidification of a Binary Eutectic Alloy: a) Equilibrium Diagram; b) Freezing Range

A binary aluminum alloy, such as the Al-Cu alloy 2219, is a system in which the major phase is a solid solution based on aluminum, and the minor phase can form a precipitate for strengthening after suitable heat treatment. Such alloys can be represented schematically on a eutectic phase diagram, such as Fig. 1a, where C_0 represents the alloy composition, C_α is the limit of solid solubility and C_E is the eutectic composition. The phase diagram also indicates the liquidus and solidus temperatures, T_L and T_S respectively, for the different alloy compositions. Under equilibrium conditions the difference between these two temperatures, the equilibrium freezing range, is the temperature range over which solidification is expected. For a eutectic system, the freezing range first increases and then decreases as the average composition is changed from the pure metal to the eutectic, as shown in Fig. 1b.

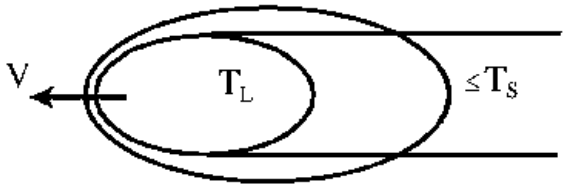

Fig. 2 Weld Pool Schematic

A schematic diagram of a weld pool moving at a velocity V is shown in Fig. 2. The isotherms for the liquidus and solidus temperatures are shown. To a first approximation the start of solidification is close to the liquidus isotherm, and solidification is completed close to the solidus isotherm. The form and spacing of solidification microstructure depends on the local thermal conditions during solidification [3,4]. Usually branched dendrites are found, with an increased volume of solid as the temperature decreases towards the solidus. Because aluminum shrinks during solidification, the volume originally occupied by the liquid above T_L is replaced by solid of smaller volume below T_S. In order to avoid the formation of cracks or voids, liquid must be fed back from the dendrite tips to make up for this shrinkage. The distance over which liquid must be fed back increases with increased

freezing range, since increased freezing range results in increased distance between the liquidus and solidus isotherms. Therefore alloys with large freezing ranges are more likely to exhibit solidification cracking during welding.

The susceptibility to solidification cracking in 6000 series alloys is high, because of a large freezing range. These aluminum alloys are based on the Al-Mg-Si system, which has a ternary eutectic (liquid to Al+Mg_2Si+Si) at about 559˚C, or 100˚C below the nominal T_L. Furthermore, aluminum alloys contain small amounts of both impurities (such as Fe) and intentional alloying additions (such as Mn and Cu). These complicate the solidification sequence and may further increase the freezing range. The solidification sequence in cast samples of the alloy 6111 (which is closely related to 6013 and 6056) has been predicted [5]. Besides the ternary eutectic at 559˚C, other eutectics were observed at temperatures of 536, 529, 508 and 487˚C, all of which involved phases high in Cu. Therefore the addition of copper to 6013 and 6056 for increased strengthening may increase the susceptibility to solidification cracking.

Filler metal additions rich in either Mg (as in 5556) or Si (as in 4043 or 4047) are used to shift the weld metal composition towards less crack sensitive compositions.

A partially molten region also is expected. Various phenomena can occur in this region which may be of concern. The partially molten region will be formed at the periphery of the weld, where the maximum temperatures lie between T_L and T_S.

The solidus of the filler metal may be above or below that of the base metal. When Al-Mg filler metals are used, the weld metal equilibrium solidus temperature is predicted to be above that of the base metal when the filler metal dilution by the base metal is between approximately 50 to 95%. For this dilution range, if sufficient stress is applied during welding, the last liquid will be in the partially molten zone and cracking will occur there instead of in the weld metal. Gittos and Scott [6] have suggested that this is the explanation for liquation cracks sometimes observed in GMA welds of 6061 using the Al-Mg filler alloy 5356. Cracks appearing to be of the liquation type have been recently reported in CO_2 laser welded blanks of 6061 using an Al-Mg-Sc filler metal [7].

Observations of precipitate-free (or dispersoid-free) zones on one side of phases at grain boundaries have been reported in laser welds of 6056 aluminum made with 4047 filler metal. Meyer et al [8] comment that the phenomenon is most noticeable near the mid-plane of the sheet. Meyer et al reported that SEM- EDX analysis of the phase revealed that it was high in silicon, but its narrow width would make accurate SEM/ EDX analysis almost impossible. They proposed that solid state grain boundary migration occurs, with small (100 to 200 nm) precipitates or dispersoids dragged by the grain boundaries. Kou [4] has suggested an alternative mechanism involving asymmetric re-solidification of the melted grain boundary liquid, with the colder base metal causing precipitate-free zones on the side of the liquated grain boundary that solidifies first. The possible importance of these findings lies in the fact that at fast welding speeds a precipitate-free or dispersoid-free zone may result adjacent to grain boundaries with a high fraction of a second phase, possibly influencing corrosion and mechanical properties of this thin region.

The 6000 series alloys use precipitation of an intermetallic phase containing Mg+Si as a strengthening mechanism. In simple ternary Al-Mg-Si alloys the precipitation hardening is based on Mg_2Si. Achievement of peak strength entails two stages of heat treatment. First, the material is soaked at a high temperature close to the melting temperature (the solution heat treatment) to dissolve solutes. Quenching from the solution temperature creates a supersaturated solution of alloying ingredients in the Al lattice, and in this condition (the W condition) the material is soft. Subsequent heat treatment at a much lower temperature (the aging heat

treatment) facilitates clustering of solute atoms and eventually formation of ultra-fine semi-coherent precipitates. The maximum hardening is found for very small precipitates (~4 nm) of nonequilibrium phases [9]. A sequence of different phases can occur, depending on the composition and aging temperature [4,8]. Aging to peak strength is identified as the T6 condition. Excessive aging time or temperature causes precipitate coarsening with attendant strength loss, commonly known as overaging or T7. If the material is left to age naturally at room temperature after solution heat treatment some incipient solute clustering and strength increase will occur - this condition is denoted T4.

Copper is added to 6000 series alloys to increase the peak aged strength above that achievable with Mg+Si alone [10]. Sufficient copper changes the main precipitating species from Mg_2Si to a quaternary intermetallic, i.e. $Al_xMg_ySi_zCu_w$ [9,10].

After welding, some natural aging will occur at room temperature, leading to partial strength recovery in the area of full prior precipitate dissolution. Strengthening arising from re-precipitation is expected to be least efficient at the outer edge of the former precipitate-free zone, where partly dissolved precipitates still exist. Thus, after welding and natural aging, a minimum of hardness and strength is normally seen at an intermediate position in the HAZ, corresponding to the location where the prior precipitate is almost fully dissolved. Artificial aging of the weldment to either the peak aged or the overaged condition after welding can be expected to be beneficial in reducing the depth of the strength valley in the HAZ.

In investigations on 6061 alloy, Hirose et al [11,12] found as-welded hardness patterns in both GTA and laser welds very similar in dimensions and minimum hardness to Grong's predictions [2]. In the GTA welds, a deficient hardness recovery was observed upon post-weld aging heat treatment, at the location corresponding to partial reversion of prior precipitates (i.e. consistent with the Grong model). However, in the same material when laser welded, post-weld aging at 175˚C was able to recover strength and hardness to nearly T6 value throughout the HAZ [11]. That is, the age-hardening-resistant zone predicted by Grong was not observed. A similar effect of low heat input laser welding was documented by Kou [4].

Laser weldments on 6013 for Daimler-Benz showed a minimum HAZ hardness of 100 HV after thorough natural aging [13]. A similar hardness pattern has been reported by Martukanitz [14] in laser welds of 6111. It is not clear why the very soft zone predicted by Grong is apparently absent. The finding of Hirose for 6061 [11] that HAZ hardness in laser welds can be almost fully recovered by artificial aging probably also applies to the higher Cu alloys.

The corrosion of welds in Al-Mg-Si-Cu alloys involves several aspects of the microstructure, as well as the filler metal and dilution. In general it appears [15,16] that Al-Si fillers do not corrode when used as fillers for 6000 alloys, but Al-Mg fillers are more subject to corrosion. This is consistent with Mg being more anodic than the other elements. Holroyd [17], on the other hand, suggests that the filler metals used for 6000 series alloys are anodic compared to the HAZ.

Complex thermal and mechanical processing has been proposed by Davydov et al [18] to achieve improved base metal mechanical properties while retaining good corrosion resistance. No work has been reported on the influence of welding after such heat treatments.

Dif [16] has reported that it is preferable to weld in the T4 condition, perhaps because of better formability, and then to overage to the T7 condition to prevent intergranular corrosion. However, this recommendation is apparently based on GMA welding.

It is well known that porosity caused by hydrogen evolution during solidification is a problem in aluminum welding. Hydrogen originating from moisture or organic contaminants is readily absorbed into the molten pool, so manufacturing processes must be

designed to exclude contaminants or to clean them from parts prior to welding.

Work at the University of Waterloo [19,20] on sheets of 5182 and 5754 alloys, using high power Nd:YAG lasers, has revealed very little porosity in bead on plate (BOP) full penetration welds for sheets wiped with methyl ethyl ketone. However, BOP welds just at the limit of full penetration contained more porosity at the weld roots [19]. This is consistent with work [21] showing higher porosity levels with unstable keyholes close to full penetration BOP Nd:YAG laser welds on 5182 and 5754 alloy sheet. Sheared edges can have debris smeared into the sheared surface, especially if the shear is not clean. Martukanitz and Smith [22] reported mechanical scraping of sheared edges and solvent degreasing prior to welding. Douglass et al [23] reported that chemical cleaning with trichlorethane, acetone and methanol was inadequate, and that porosity dropped significantly when most of the oxide was removed, by brushing or a commercial aluminum deoxidizer. They obtained best results by using the deoxidizer, brushing, and then degreasing with all of the above solvents (trichlorethane, acetone and methanol).

3. Production Process

Butt welds in 1.6 mm thick Alcoa 6013-T4 aluminum alloy sheet were produced using a 4.3 kW Trumpf Nd:YAG laser. Filler wire additions were used in all welds. Aluminum filler alloys 4043, 4047 and 5556 were evaluated. Welding was performed at a speed of 6.2 m/min, with a filler wire feed rate of 4.0 m/min. Ar shielding gas was applied on the beam side only. Completed weldments were square in planform, approximately 30 cm on the sides. The weld, parallel to an edge, bisected the weldment. Strips approximately 2.5 cm wide were cut perpendicular to the weld for subsequent testing. Specimens used for strength testing were heat treated after welding to the peak aged temper using the process described in [24].

4. Experimental & Investigative Procedures

Tensile tests were performed on flat transverse specimens at room temperature per ASTM E8-99 using an Instron testing machine. Elongation was measured using an MTS Model 652.11B-20 extensometer with a calibrated gauge length of 25.4 mm. Microhardness measurements were taken using a Leitz Wetzlar Vickers MINILOAD microhardness tester.

Optical and scanning electron microscope (SEM) examination of weld surfaces and tensile test fracture surfaces was carried out on coupons in the as-received condition. For SEM examination, portions of selected weldments were first removed by manual saw cutting to generate offcuts small enough to load into the microscope chamber (~10 mm square or smaller). Most SEM offcuts were washed in acetone and dried before insertion into the microscope, to reduce charging problems caused by any nonconductive particles lying on the surface.

Specimens for optical microscopy and SEM/ EDXA microanalysis were first manually saw cut and mounted in cast cylindrical cold-setting resin mounts to facilitate handling during polishing and etching. Metallographic preparation followed conventional practice: wet grinding on successively finer silicon carbide papers up to 1200 grit, followed by mechanical polishing using 6μm and 1μm aqueous diamond slurries and short nap cloths. Most specimens were prepared using a Struers mechanized polishing apparatus; however, some refinishing was done manually. Finishing with 1μm alumina in aqueous slurry was also found to be feasible, but was not generally practised because the softer medium left greater phase-to-phase relief on specimen surfaces.

Specimens for EDXA were examined in the as-polished condition to reduce measurement errors related to selective phase removal by etch attack.

Specimens for optical examination of prepared sections were etched after polishing using one or more of the following etching solutions: Aqueous 0.5% HF; Kellers Reagent, and Graff

& Sargent Reagent [25]. The 0.5% HF etchant provided light staining of intermetallics with little or no attack of the alpha aluminum phase. It permitted general categorization of weld zones but was not responsive to local variations in solute content so provided little insight into the solidification process. Kellers reagent revealed solidification and liquation structures in great detail but was very prone to pitting unless made fresh with deoxygenated water. The Graff & Sargent etch was designed to level and activate polished surfaces, and was found very useful as the first stage of a two step etching sequence ending with Kellers reagent.

5. Weldment Tensile Strength

The strength properties of the weldments were measured using flat transverse tensile specimens at room temperature, after post-weld aging heat treatment (PWHT). Nominal failure stresses were approximately 80% of the base metal UTS in the peak aged temper. A typical plot of stress versus strain is shown in Fig. 3.

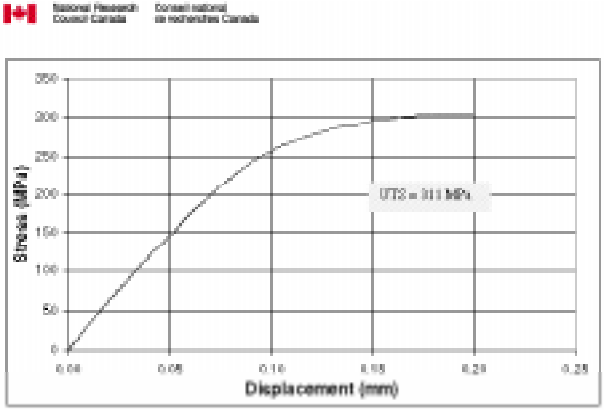

Fig. 3 Tensile Test Results for 6013 Weldment with 5556 Filler Wire & PWHT

Tensile test coupons displayed a consistent fracture appearance, with a single ductile shear failure surface located entirely in fused weld metal and with a shear angle of about 50˚ to the plane of the sheet. At high magnification, fracture surfaces displayed ductile dimpling that corresponded closely with the dendritic solidification structure, with interdendritic particles acting to nucleate microvoids during shear deformation.

None of the broken tensile specimens showed any evidence of plastic deformation or tearing in any part of the PMZ or HAZ. All of the tensile fracture paths appeared to remain entirely within the weld fusion zone. Nominal elongations were small, although this does not necessarily imply that the welds were brittle. Observations show that most of the deformation near failure takes place within the narrow width (~2 mm) of the fusion zone, whereas the nominal strain is calculated over the largely unyielded gauge length.

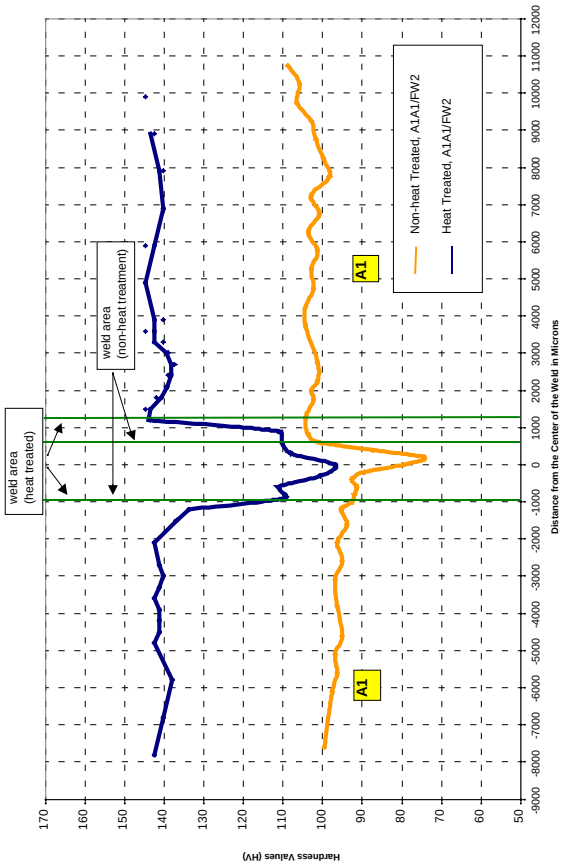

Fig. 4 Hardness Values vs. Distance Weld Centre Line, 6013 Weldment with 4047 Filler Wire

6. Microhardness Profile

Fig. 4 shows the hardness profile for a typical weldment before and after aging PWHT. The minimum hardness was observed at approximately the weld centre line. The hardness increase after PWHT away from the HAZ is due to the change of temper from T4 to T6. There is also a significant increase in

hardness within the fusion zone, indicating a partial strength recovery due to the aging PWHT. During welding, the filler metal and base metal combination are fused, leading to complete dissolution of the constituent elements. This is followed by a rapid solidification similar to the quench of a solution heat treatment. The PWHT apparently results in some level of precipitation hardening of the base metal-filler alloy blend.

Microhardness testing disclosed no evidence of local strength reduction in the PMZ.

7. Cracking

The fusion and partially molten zones of the fractured tensile specimens were examined for evidence of discontinuities. In addition, specimen deformation and fracture mode, in relation to the microstructure and apparent weld metal composition, were determined.

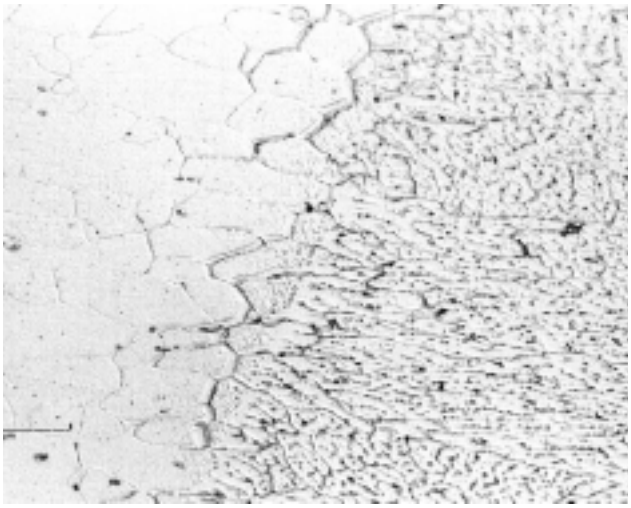

Fig. 5 Fusion Boundary Area (6013 with 4043 Filler Wire) Showing Growth of Dendritic Structures

All the welds displayed a very normal development of the solidification microstructure, which was generally consistent with previous observations of solidification structures in arc and laser welds. Furthermore, except for some differences in the incidence of weld defects, coupons from all weldments displayed similar microstructural development. As is normal with weld solidification, freezing began with planar epitaxial growth from the solid (Fig. 5), which broke down within about 2 microns into bundles of columnar cellular dendrites growing approximately normal to the local solid/liquid interface.

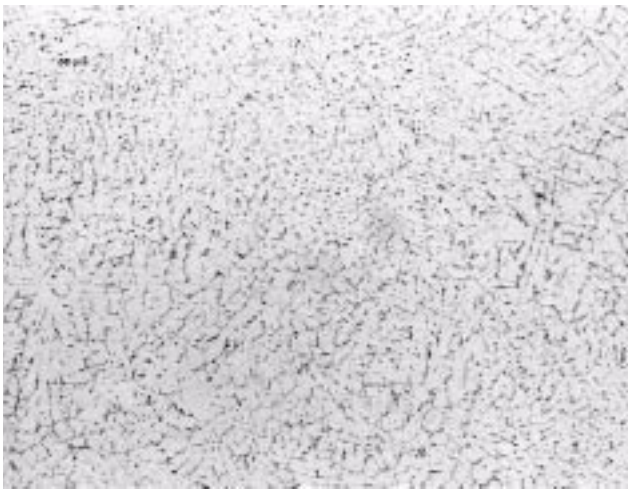

Fig. 6 Transition from Columnar to Equiaxed Dendrites near Weld Centreline (6013 with 5556 Filler Wire)

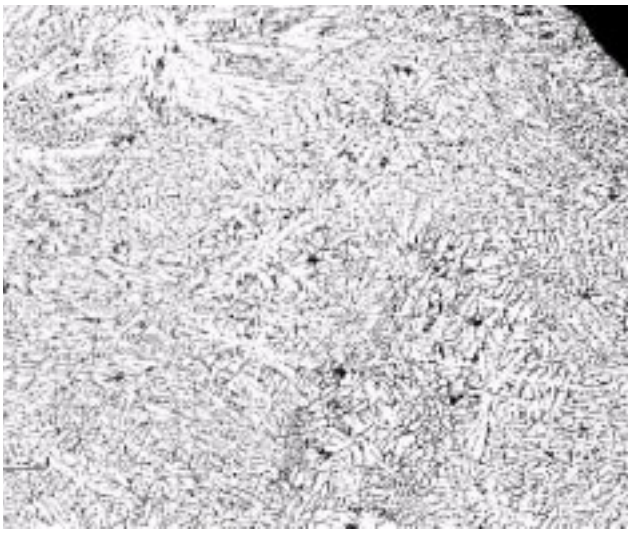

Fig. 7 Bundles of Equiaxed Dendrites between Columnar Growth near Weld Centreline (6013 with 4043 Filler Wire)

The dendritic growth micro-segregation was completed by growth of a different solid phase or a eutectic from the solute-enriched liquid between the dendrites. All welds also had a significant population of true equiaxed grains, representing up to one third of the weld cross section. These normally nucleate and grow in the

liquid at the tail of the weld pool and are randomly oriented. The equiaxed grains were clearly distinguishable from the columnar epitaxial grains as the former had coarser dendrite arm spacing and more dendrite side-branching, see Figs. 6 and 7.

All the welds had an interdendritic substructure following the above pattern. Dendrites were consistently outlined with a row of fine platelets of the dominant eutectic second phase, either Si or Al_3Mg_2.

None of the welds had a sufficient rate of filler metal addition to place their net composition outside the range of high solidification crack susceptibility. No longitudinally oriented cracking has been found in any of the weld coupons. However, many of the coupons showed some evidence of microcracking in a plane transverse to the welding direction when subjected to preliminary optical macro examination of their tensile fracture surfaces. An SEM image of typical crack appearance is shown in Fig. 8. To understand these fissures in relation to the microstructure, metallographic sectioning and preparation was carried out in plan view (section plane parallel to the sheet surface). Since these cracks were oriented normal to the sheet surface and hence parallel to the usual transverse metallographic section, the probability of seeing them using the latter section orientation was very small.

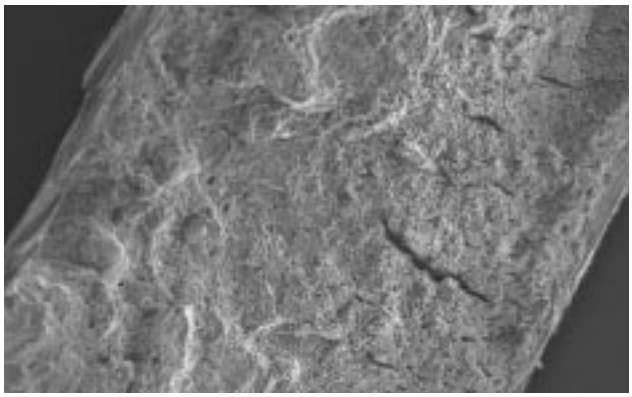

Fig. 8 View of Fracture Surface Showing Solidification Fissures (6013 with 4047 Filler Wire)

Fissures visible on the tensile fracture surfaces were found to be interdendritic, usually intergranular, solidification microcracks in the columnar dendritic microstructure. Welds made using AA5556 and AA4043 filler wire had roughly similar populations of microcracking and had significantly more microcracking than welds using AA4047.

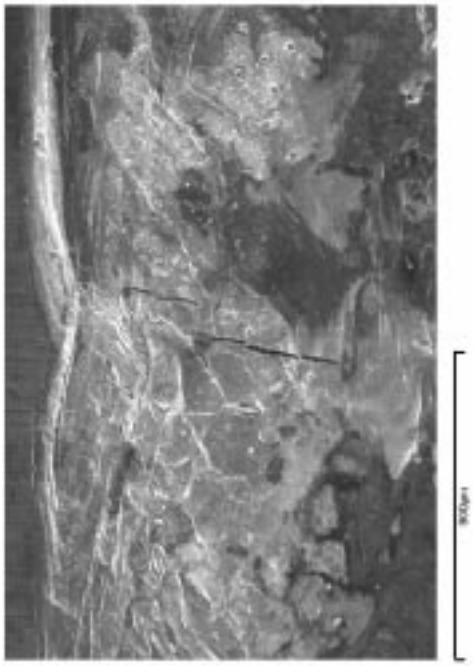

Fig. 9 Intergranular Solidification Crack Parallel to Local Dendritic Growth (6013 with 5556 Filler Wire)

On the tensile specimen fracture surfaces and in plan view optical metallography, the columnar microcracks were seen predominantly in the half of the coupon thickness closest to the weld root surface. This led to a search for evidence (using EDX analysis) of incomplete mixing of filler metal), but such evidence was not found. Two independent forms of confirmation have been obtained that significant quantities of these small transverse cracks are not confined only to the root region and may grow to larger size, actually intercepting either the front or root surface of the weld in some specimens. Nondestructive evaluation of some weldments [26] has shown interesting families of transverse crack indications. Also, instances of transverse solidification cracks which had propagated to the

front/top weld surface have been seen using the SEM, as shown in Fig. 9.

Cracks in intact specimens were very tight and in some cases quite hard to distinguish metallographically from uncracked grain boundaries. Apparently, the lateral contraction accompanying plastic deformation during tensile testing opened the cracks in the specimens used for tensile testing, making them much easier to see.

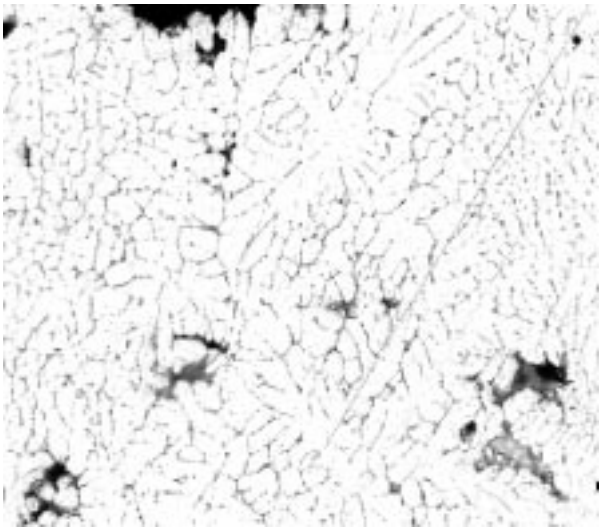

Fig. 10 Interdendritic Shrinkage Cavity (6013 with 5556 Filler Wire)

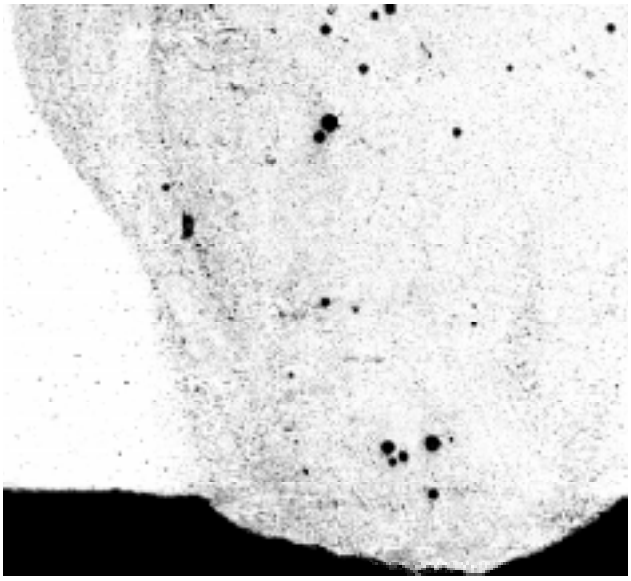

Fig. 11 Example of Excessive Porosity (6013 with 4047 Filler Wire)

In addition to these oriented columnar microcracks, the equiaxed solidification zone of all coupons examined displayed at least sporadic randomly oriented interdendritic shrinkage cavities. Typical appearance of such cavities is illustrated in Fig. 10. Relatively dense arrays of such cavities were occasionally encountered. The morphology of these discontinuities was very similar, except for the scale of both microstructure and cavities, to shrinkage cavities typically found in the final regions to freeze of aluminum castings [1]. The freezing of a liquid aluminum alloy is accompanied by a volumetric shrinkage of about 5% on phase change, so that freedom from discontinuities requires continuous feeding of liquid between the dendrites from the molten weld pool. Insufficient solute content in the liquid and low local temperature gradient lead together to difficulties with liquid feeding so that some of the volumetric shrinkage is made up by cavitation. Tensile strains are not required. Solidification shrinkage cavitation provides additional evidence of insufficient filler metal content in these weldments, leading to an excessive freezing range.

8. Porosity

With one significant exception noted below, all weld coupons and metallographic sections were remarkably free of fusion zone gas porosity. This indicates that the basic cleaning and process technology to make the coupons was appropriate. One set of weldment coupons displayed extensive, unacceptable amounts of gas porosity on all sections examined, see for example Fig. 11. This particular coupon was most probably contaminated or improperly cleaned prior to welding.

Gas pores were observed in liquated grain boundaries in the partially molten zone, see Fig. 12. The gas causing these pores was clearly liberated from the base metal during liquation, indicating that the base metal was inadequately degassed by the manufacturer during the slab casting process.

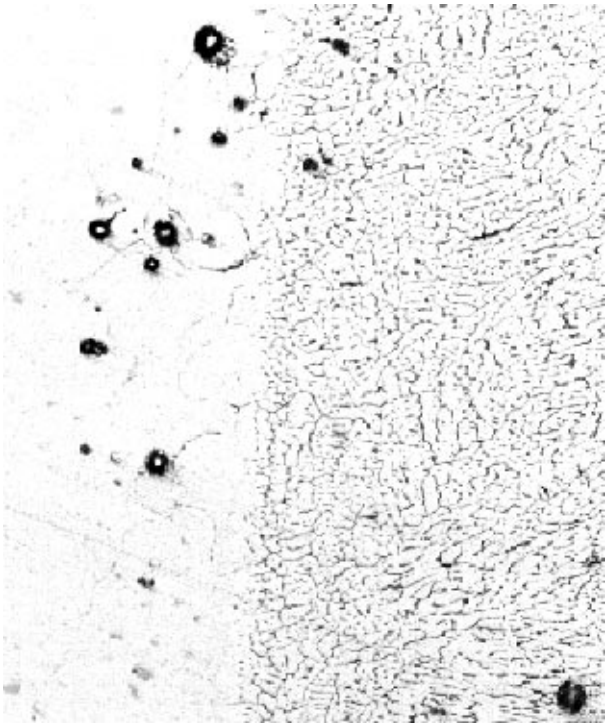

Fig. 12 Gas Pores at Fusion Boundary (6013 with 4047 Filler Wire)

9. Fusion Boundary & Partially Molten Zone

A significant partially melted zone (PMZ) was present in all coupons and the morphology of this zone was similar across all the weldments. The extent of the PMZ was approximately 2 to 3 grain diameters (~60 μm) from the fusion boundary. Transient melting followed grain boundaries in the solid and also tended to envelop dispersoids occurring within the grains in the zone, Fig. 13.

Transiently liquated grain boundaries showed asymmetric re-solidification as in [4], with a dispersoid-free zone on the cold side of the boundary and eutectic particles all deposited on the side of the grain boundary that was expected to freeze last, Fig. 14.

No weldment discontinuities were found in any coupon in, or associated with, the transiently liquated zone. Furthermore, the interdendritic solidification cracking found in the weld fusion zone was not found to extend near or into the partially molten region in any specimen examined.

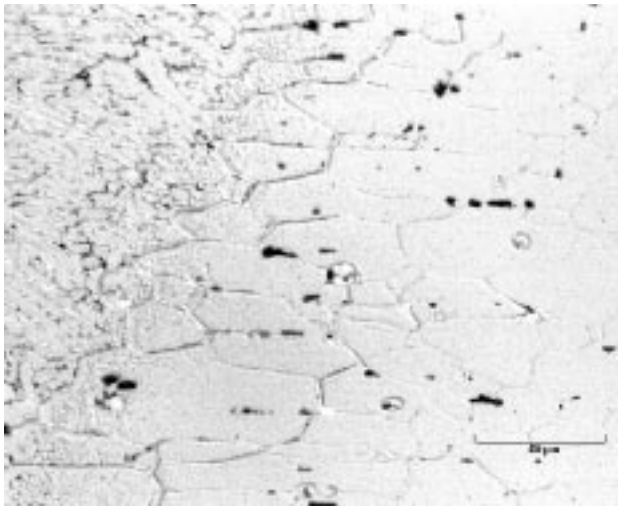

Fig. 13 Results of Transient Liquation Around Dispersoid Particles

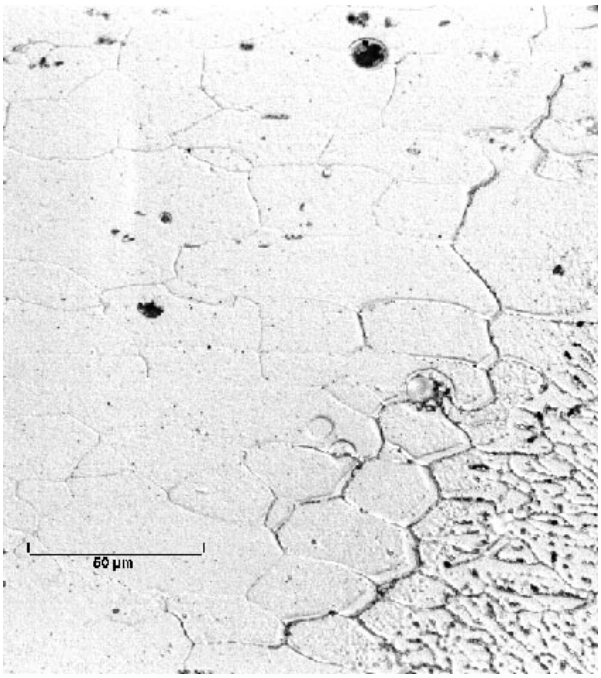

Fig. 14 Asymmetric Deposition of Eutectic Phases during Grain Boundary Re-Solidification

Therefore, although the welding process evidently produces a transiently liquated structure susceptible to rupture, the thermomechanical response of the solid material surrounding the travelling weld pool apparently generates little or no tensile strain field in the affected area until after the local temperature has decreased below the solidus.

10. Corrosion Resistance

Laser welded aluminum specimens were submitted for evaluation of intergranular corrosion resistance. All of the specimens were subjected to PWHT from T4 to T6. Each sample was immersed in a sodium chloride and hydrogen peroxide solution per ASTM G110 for 24 hours. The samples were sectioned, prepared metallographically and examined for the presence of intergranular corrosion in the weld and base materials. All samples were etched in Kellers reagent prior to examination. Intergranular corrosion was evident in both the base metal and the welds of all specimens, comparable to that of a 7075-T6511 control specimen. No selective attack in the welds was observed.

11. Unmelted HAZ & Base Metal Structure

No microstructural changes were seen in the HAZ beyond the extent of the PMZ. Therefore, the full extent of the HAZ has been studied by using microhardness data to estimate the nature of thermally induced metallurgical changes as a function of distance from the weld fusion zone.

12. Discussion & Conclusions

Qualitative chemical analysis by EDXA suggested that significant loss of Mg occurred due to vaporization in all welds. However, the inherent accuracy of this measurement technique for low concentrations of Mg in Al was found to be inadequate for estimating either dilution or the extent of vaporization loss.

The recommended filler metal addition rate for future weld trials is at least twice the rate used in the welds examined, based on the use of 4047 filler metal.

All welds displayed a normal dendritic solidification microstructure beginning at the fusion boundary as epitaxial columnar grains, consistent with prior experience with the alloys involved. All welds had a significant zone of true equiaxed solidification structure, occupying up to the middle third of the fused cross section. The equiaxed grains displayed a larger dendrite arm spacing than the columnar regions, consistent with softer regions in the central regions of several weld metal cross sections.

All welds displayed some intergranular solidification cracking in the columnar solidification zone, with the crack planes normal to the sheet surface and nearly normal to the welding direction. Cracks appeared to be predominantly located in the bottom (root) half of the welds but were also seen at the top surface. Qualitative comparison suggested that cracking was less frequent in the welds made with 4047 filler compared to those made with 4043 or 5556, which is consistent with predictions of previous investigators for the observed dilutions.

Small sporadic non-oriented interdendritic shrinkage cavities were also seen in the equiaxed zone in most weldments. These resembled the shrinkage cavities often found in aluminum alloy foundry castings, and provided additional confirmation of systematically excessive base metal dilution. Dense arrays of such cavities were found only in welds made with 4043 or 5556 filler. No longitudinally oriented solidification defects were found in any weldment. That is, neither link up of shrinkage cavities nor reorientation of transverse columnar cracks was observed.

Most weldments appeared essentially free of gas porosity in the fusion zone. Only one weld had excessive porosity. Gas pores were seen in liquated grain boundary areas of the partially molten zone of several weldments, suggesting that the base metal was manufactured with an excessive hydrogen content.

The heat-affected zone of all welds showed a significant area of partial melting, primarily at grain boundaries and dispersoid particles, immediately adjacent to the fully molten zone. The width of the PMZ was generally two to three grain diameters. Re-solidification of liquated material was asymmetric as suggested by previous investigators, with second phase (eutectic) material in the last-to-freeze location. Farther out in the heat-affected zone, beyond the area of liquation, no microstructural changes due

to the welding thermal cycle were visible by optical microscopy.

Liquation cracking was not observed in any weld section examined, nor was any solidification crack seen to run near or into the fusion boundary region. Similarly, no indication was seen of significant deterioration of mechanical properties specifically related to the liquation and re-solidification in the PMZ.

Average weldment tensile strengths showed reasonable correlation with weld metal microhardness as measured on post-weld aged specimens.

References

[1] G.F. Vander Voort, Metallography Principles and Practice, McGraw-Hill, 1984, Chapter 5.

[2] O. Grong, Metallurgical Modelling of Welding, The Institute of Materials (Cambridge University Press), 1994

[3] W. Kurz and D.J. Fisher, Fundamentals of Solidification, 3rd Ed., Trans Tech Publications, Aedermannsdorf, Switzerland, 1992

[4] S. Kou, Welding Metallurgy, Wiley, New York, 1987

[5] X.-G. Chen and J. Langlais, Materials Science Forum, Vols 331-337, 215-222, 2000

[6] N.F. Gittos and M.H. Scott, Weld. J., Vol. 60, 95-s to 103-s, 1981

[7] S. Bhandari and J. Mazumder, Laser Apps. Auto Industry - ICALEO 2000, Laser Inst. America (LIA), Orlando, FL., Vol. 91, paper B-30, 2000.

[8] B.C. Meyer, H. Doyen, D. Emanowski, G. Tempus, T. Hirsch and P. Mayr, Met. Mater. Trans. A, vol. 31A, 1453-1459, 2000.

[9] M. Tanaka and T. Warner, Mat. Sci. Forum, Vols. 331-337 ,983-988, 2000.

[10] R. Dif, D. Bechet, T. Warner and H. Ribes. Proc. 4th Int. Conf. on Aluminum Alloys, 1998.

[11] A. Hirose, H. Todaka and K.F. Kobayashi, Met. Mater. Trans., Vol. 28A (12), 2657-2662, 1997.

[12] A. Hirose, H. Todaka et al, Met. Mater. Trans., Vol. 30A (12), 2115-2120, 1999.

[13] L.A. Guitterez, G. Neye and E. Zschech, Weld. J, Vol. 75, 115-s to 121-s, 1996.

[14] R.P. Martukanitz, D.J. Smith et al., Laser Beam Welding of Aluminum Alloys for Automotive Applications, Paper Presented at SAE International Congress, Detroit MI, 1994.

[15] J.E. Hatch (Editor), Aluminum Properties and Physical Metallurgy, ASM International, Metals Park OH, 1984.

[16] R. Dif, (Pechiney), Private Communication, 2000.

[17] N.J.H. Holroyd, Conf. Proc. - Environment-Induced Cracking of Metals, National Association of Corrosion Engineers, Houston, TX, 311-345, 1989.

[18] V.G. Davydov, V.S. Siniavski et al., Mat. Sci. Forum, Vols. 331-337, 1315-1320, 2000.

[19] M. Deutsch, MASc candidate, University of Waterloo, private communication, 2000.

[20] A. Punkari, MASc candidate, University of Waterloo, private communication., 2000.

[21] M. Pastor, H. Zhao, R.P. Martukanitz and T. Debroy, Weld. J. Vol. 78 (6), 207-s to 216-s, 1999.

[22] R.P. Martukanitz and D.J. Smith, 6th Int. Conf. On Aluminum Weldments, 309-323, AWS, Miami, FL. 1995.

[23] D.M. Douglass, J. Mazumder and K. Nagarathnam, Trends in Welding Research, (ed. H.B. Smartt, J.A. Johnson, S.A. David), 467-478, ASM International, Materials Park, OH., 1996.

[24] ALCOA Aluminum Alloy 6013, Green Letter No. 225, 1st Edition, December 1987, Stanley J. Cieslak

[25] W.R. Graff & D.C. Sargent, Metallography, 14, 1981, 69-72

[26] R. Wong, A. Ardis & K. Cunninham, Bombardier Materials Report 2001LAB08681, October 10, 2001.